metals

MDPI

Article

Effect of the Gas Temperature on Agglomeration of Au Nanoparticles Synthesized by Spark Discharge and Their Application in Surface-Enhanced Raman Spectroscopy

Denis Kornyushin, Andrey Musaev, Anton Patarashvili, Arseny Buchnev, Pavel Arsenov, Matthew Ivanov, Olesya Vershinina, Ekaterina Kameneva, Ivan Volkov, Alexey Efimov * and Victor Ivanov

Moscow Institute of Physics and Technology, National Research University, 141701 Dolgoprudny, Russia
* Correspondence: efimov.aa@mipt.ru

Abstract: In this work, we have, for the first time, experimentally verified the hypothesis of reducing the agglomeration rate of aerosol nanoparticles produced by spark discharge upon decreasing the carrier gas temperature in the range of 24 °C to –183 °C. The synthesis of nanoparticles was implemented as a result of spark ablation of electrodes manufactured from Au with a purity of 99.998% installed in a specially designed gas chamber dipped into liquid nitrogen (−196 °C) to cool down the carrier gas supplied through one of hollow electrodes. It follows from the analysis of transmission electron microscopy images that both the average size of primary nanoparticles and the degree of their sintering become lower if the gas is cooled. For example, in the case of using nitrogen as a carrier gas, the average size of primary nanoparticles decreases from 9.4 nm to 6.6 nm as the gas temperature decreases from 24 °C to –183 °C. This also causes the aggregates to become more branched, manifested by the reduction in their solidity from 92% to 76%. The agglomeration model of Feng based on Smoluchowski theory was employed to calculate particle size distributions that were found to be consistent with the experimental data. The gold nanoparticles synthesized at room and cryogenic temperatures of the carrier gas (N_2, Ar + H_2, He) were used to pattern plasmonic nanostructures on ceramic alumina substrates by using aerosol jet printing technology for the purpose of demonstrating the possibility of their application in surface-enhanced Raman spectroscopy (SERS). The SERS enhancement factor was estimated at 2×10^6 from the analysis of SERS and normal Raman spectra of 1,2-bis(4-pyridyl)ethylene used as an analyte.

Keywords: aerosol nanoparticles; agglomeration; spark discharge synthesis; gold; SERS; aerosol jet printing; Raman spectroscopy

Citation: Kornyushin, D.; Musaev, A.; Patarashvili, A.; Buchnev, A.; Arsenov, P.; Ivanov, M.; Vershinina, O.; Kameneva, E.; Volkov, I.; Efimov, A.; et al. Effect of the Gas Temperature on Agglomeration of Au Nanoparticles Synthesized by Spark Discharge and Their Application in Surface-Enhanced Raman Spectroscopy. *Metals* **2023**, *13*, 301. https://doi.org/10.3390/met13020301

Academic Editors: Zhifeng Wang and Qibo Deng

Received: 30 December 2022
Revised: 19 January 2023
Accepted: 30 January 2023
Published: 1 February 2023

1. Introduction

The generation of nanoparticles using the electrical erosion of electrodes in gas is a relatively facile, scalable, and material-universal synthesis method [1,2]. This method is widely used to obtain aerosol nanoparticles and mix them [3,4] with further application in spectroscopy [5,6], printed electronics [7,8], and functional coating [9]. The features of this method are the chemical purity and the small size of the synthesized nanoparticles (less than 10 nm), and clusters containing up to tens of atoms [10]. However, after generation, the primary nanoparticles inevitably rapidly agglomerate, which can be a limiting factor for many applications. This paper challenges this paradigm by providing experimental evidence that agglomeration can be controlled by controlling the temperature of the carrier gas. Thus, it is possible to limit the cooling rate and Brownian motion of the nanoparticles, and synthesize either aggregates or agglomerates [11]. The nanoparticles tend to aggregate and agglomerate, due to the attraction between nanoparticles such as van der Waals forces and chemical bonds [12]. Both aggregation and agglomeration are assemblies of nanoparticles, where aggregation includes strong and dense colonies of particles, but

agglomeration comprises loosely combined particles that can be disrupted by mechanical forces [13]. Aggregates or agglomerates of nanoparticles are known to be preferred in applications such as catalysts [14–16] or sensors [17–20] because they have a large surface area. However, such particles are unsuitable for use as building blocks of conductive structures because they cause various problems such as low packing density and low electrical conductivity.

Many researchers have developed methods for reducing agglomeration [21,22]. Tabrizi et al. investigated the agglomeration of nanoparticles by varying the energy per spark, flow rate, and type of carrier gas [23]. Han et al. presented an asymmetric pin-plate electrode geometry that provides much faster particle transfer from the spark discharge zone [24]. Changing conditions, such as further thermal or laser sintering, can also lead to a reduction in agglomerates and the formation of larger and single nanoparticles [25,26]. It was shown in [27] that agglomeration can be reduced by unipolar charging of nanoparticles, for example, using a corona charger. However, this method can be a limiting factor for the scalability of the spark discharge method.

For the first time, this article reports an experimental study of the influence of carrier gas temperature on the reduction in agglomeration of Au nanoparticles synthesized using a spark discharge. A sealed gas-discharge chamber capable of operating in liquid nitrogen was developed specifically for these experiments. The size and morphology of primary nanoparticles and their agglomerates were studied using transmission electron microscopy. In this study, a theoretical approach was also applied to predict the particle size distribution as a function of gas temperature. To this end, the model of Feng et al. [28] for primary nanoparticles and classical agglomeration theory were combined with a log-normal self-conserving size distribution function. In addition, the formation of plasmonic nanostructures from aggregates and agglomerates synthesized by varying the temperature and type of carrier gas was performed. The obtained structures from Au nanoparticles were investigated for applications in Raman spectroscopy with surface enhancement. This direction is promising for the rapid production of economical and chemically pure nanostructures for Raman spectroscopy [18,29].

2. Materials and Methods

2.1. Synthesis of Nanoparticles in a Spark Gas Discharge

Figure 1 shows a setup for the synthesis of gold nanoparticles in a cooled gas atmosphere. The setup was a hermetically sealed gas-discharge chamber located inside a 10 L plastic thermobox filled with liquid nitrogen (T_b = –196 °C). Details on the design and electrical circuit of the gas-discharge chamber have been described earlier [30,31]. The carrier gas was supplied to the synthesis chamber through a cooled coil placed in liquid nitrogen. Three types of gases (N_2, Ar + H_2, and He) were used in the study for the synthesis of nanoparticles in a spark discharge. The carrier gas temperature T_{gas} was measured at the chamber outlet using a k-type thermocouple (MT1/T-K/3.0–250, FuehlerSystems, Germany). At the same time, the gas temperature was controlled by changing the level of liquid nitrogen poured into the thermobox in the range of 24 °C to −183 °C. Because the chamber had a tube outlet above the liquid nitrogen surface (see Figure 1), the minimum gas temperature (−183 °C) was just above the boiling point of nitrogen (−196 °C).

In turn, the synthesis of nanoparticles was carried out in the process of electrical erosion between gold electrodes with a mass fraction of Au of about 99.9981%, with a gap distance of 0.5 mm. In order to limit the agglomeration of particles, the values of the energy and repetition rate of the discharges were chosen to be minimal and amounted to 7 mJ and 10 Hz. Discharge voltage waveforms were monitored using a digital oscilloscope (DS6102, Rigol Technologies, Beijing, China). The space between the electrodes was constantly blown with a "cold" carrier gas at a flow rate of 1–10 L/min, which removed the erosion products of the electrodes from the gap.

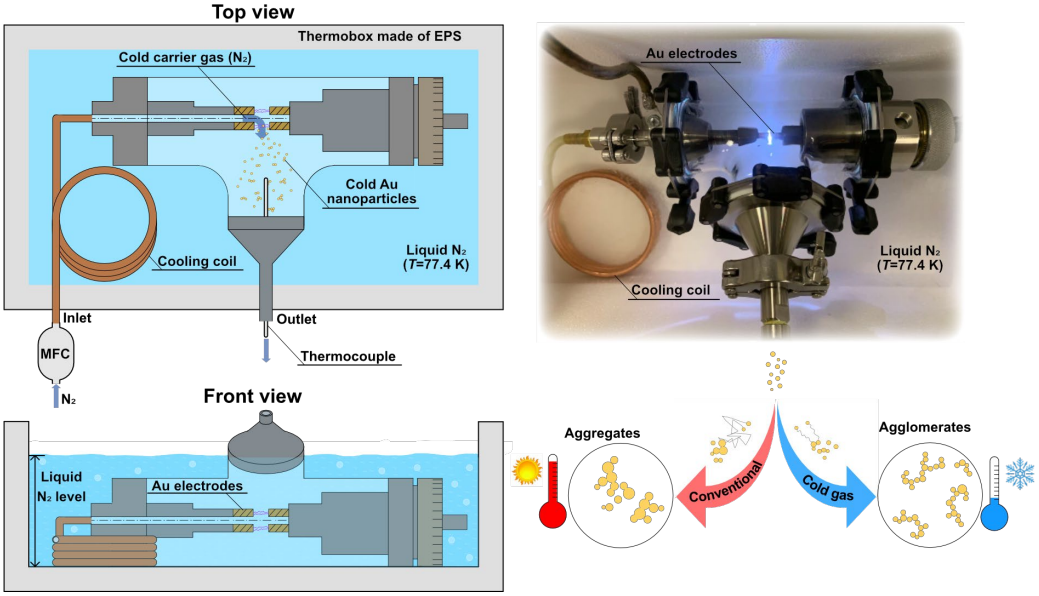

Figure 1. Image of the experimental setup for the synthesis of nanoparticles in cold gases (N_2, Ar + H_2, and He) by spark discharge using a sealed gas-discharge chamber immersed in liquid nitrogen ($T = -196$ °C).

2.2. Study of the Size and Morphology of Primary Nanoparticles and Their Agglomerates

The morphology and size of the synthesized nanoparticles depending on the temperature of the T_{gas} carrier gas were studied using a transmission electron microscope (TEM) (JEM-2100, JEOL Ltd., Tokyo, Japan). It should be noted that the TEM method makes it possible to estimate both the size of primary nanoparticles and their agglomerates, and the uncertainty of the image analysis method does not exceed 5%.

The average size of the particles was determined based on TEM image analysis using a sample of 300–400 particles. Despite the non-spherical or uniform shape of the nanoparticles, the sizes of the nanoparticles were characterized by a certain equivalent diameter. The measurements were carried out by estimating the area of each particle S. The average diameter of $d_{p,a}$ nanoparticles was determined using Formula (1):

$$d_{p,a} = 2\sqrt{\frac{S}{\pi}} \quad (1)$$

For comparison with the experiment, the theoretical calculation of the size of primary particles d_p and agglomerates d_a was carried out using the Feng model [28] using Formula (2):

$$d_p \approx \left(\frac{\Delta m K V}{\rho \frac{\pi}{3} Q^2}\right)^{\frac{1}{3}} \quad (2)$$

where Δm—the mass production of nanoparticle synthesis;

K—the coagulation coefficient;

V—the effective volume near the electrode in which the formation of primary particles occurs/the effective volume of the gas path, including the volume of the chamber;

ρ—the electrode material density;

Q—the volume flow of gas.

The coagulation coefficient K, which is responsible for agglomeration, was estimated using Formula (3):

$$K = \frac{4kT_{gas}C_c}{3\eta} \quad (3)$$

where k—the Boltzmann constant;

T_{gas}—the gas temperature;
C_c—slip coefficient;
η—the dynamic viscosity of the gas.
Calculation of solidity of agglomerates was carried out according to the Formula (4):

$$\varphi = \frac{\sum S_i}{S_0} \quad (4)$$

where $\sum S_i$—the total area of particles in the agglomerate;
S_0—the area of the entire agglomerate.
This parameter makes it possible to more accurately describe the resulting agglomerates, since their size depends not only on the number and size of colliding particles, but also on the density of their placement. The particles are expected to cool faster in the cold gas, resulting in less coalescence and a more branched agglomerate structure.
Another important parameter for characterizing agglomerates is the relative bond strength of nanoparticles in the agglomerate χ. It is known that the bond strength depends linearly on the fusion area, since the number of bonded atoms increases linearly. A visual representation of particles with different values of the relative bond strength is shown in Figure 2. The relative bond strength between nanoparticles synthesized at different temperatures was calculated using the following Formula (5):

$$\chi = \frac{S_{contact}}{S_{particle}} = \left(\frac{d_c}{d_p}\right)^2 \quad (5)$$

where $S_{contact}$—the area of contact between particles;
$S_{particle}$—cross-sectional area of the particle.
Thus, the value of χ was determined as the square of the ratio of the channel width d_c between particles to their average diameter d_p.

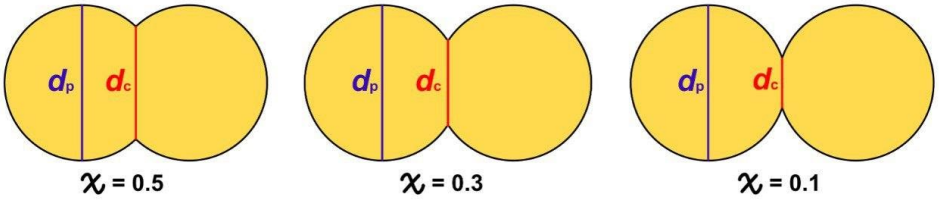

Figure 2. Image of particles with different values of relative bond strength.

2.3. Mass Production Rate of Nanoparticle Synthesis

The mass production rate of nanoparticle synthesis was evaluated using the gravimetric method by changing the mass of the electrodes using analytical scales (Secura 225D-1ORU, Sartorius Inc., Göttingen, Germany). In addition, using the Llewellyn Jones Equation (6), the mass production rate of nanoparticle synthesis was theoretically estimated to determine the effect of gas temperature T_{gas} on the efficiency of electrode evaporation [32]. Thus, the mass of the evaporating material for one discharge m was calculated using the formula:

$$m = \frac{0.5c_eV^2 - bT_{gas}{}^4 - gk(T_b - T_{gas})}{c_{ps}(T_m - T_{gas}) + \Delta H_f + c_{pl}(T_b - T_m) + \Delta H_v} \quad (6)$$

where $0.5c_eV^2$—the energy of a single discharge (c_e = 38 nF, V = 600 V);
$bT_{gas}{}^4$—energy losses due to thermal radiation of the hot electrode area ($b = 2.7 \times 10^{-20}$ J/K^4, T_{gas} = 90 K (–183 °C));
$gk(T_b - T_{gas})$ —energy losses for heat transfer from the hot area of the electrode ($g = 6.9 \times 10^{-9}$ m·s, $k = 5.67 \times 10^{-8}$ W/(m^2·K^4), T_b = 3129 K (2856 °C));

$c_{ps}(T_m - T_{gas})$ and $c_{pl}(T_b - T_m)$—the specific energy for heating to the melting and boiling points, respectively (c_{ps} = 129 J/(kg·K), T_m = 1337 K (1064 °C), c_{pl} = 129 J/(kg·K));

ΔH_f, ΔH_v—specific heat of melting and vaporization, respectively ($\Delta H_f = 63.7 \times 10^3$ J/kg, $\Delta H_v = 16.5 \times 10^5$ J/kg).

Thus, multiplying the calculated mass m by the discharge repetition frequency f, it is possible to obtain the mass production rate of nanoparticle synthesis Δm (mg/h), which, in turn, affects the agglomeration of nanoparticles.

2.4. Aerosol Printing and Measurements of SERS Structures

In order to determine the effect of the carrier gas type and its temperature T_{gas} on the functional properties of nanoparticles, gold nanostructures were printed from nanoparticles obtained in argon, nitrogen, and helium at temperatures of 24 °C and −183 °C, followed by study on a Raman spectrometer. The formation of structures from Au nanoparticles in the form of 3 mm × 3 mm square pads on a ceramic substrate made of aluminum oxide was carried out using the method of "dry" aerosol printing [33,34]. Details about this method are described in previous works [35–38]. Table 1 shows the main parameters for printing surface-enhanced Raman spectroscopy (SERS) structures from Au nanoparticles obtained in various gaseous media (N_2, Ar + H_2 and He) at temperatures of 24 °C and −183 °C, respectively.

Table 1. Parameters of the formation of structures in the form of pads on ceramic substrates by dry aerosol printing.

Carrier Gas	Printing Speed v, mm/s	Nozzle to Substrate Distance WD, mm	Carrier Gas Flow Q_a, cm^3/min	Focus Gas Flow Q_{sh}, cm^3/min
nitrogen argon + hydrogen helium	10.5	3	1000	100

The formed SERS structures were thin layers of nanoparticles 100–500 nm thick. The deposition of nanoparticles was carried out through a coaxial micronozzle with an outlet diameter of 300 μm. Aerosol nanoparticles collided with the substrate at high speed (>100 m/s) and attached to its surface. The width of the nanoparticle beam was controlled by the flow rates Q_a of the carrier gas and Q_{sh} of the focus gas, respectively. The focus gas flow Q_{sh} prevented clogging of the micronozzle by limiting the expansion of the nanoparticle beam. In the presented experiments, the flows for all carrier gases Q_a and Q_{sh} were 1000 and 100 cm^3/min, respectively. For efficient deposition of nanoparticles, the distance from the micronozzle to the substrate was 3 mm. The speed of the substrate movement and the step of printing lines were chosen in such a way as to form structures with the maximum nanoparticle density. Direct formation of SERS structures in the form of 3 mm × 3 mm square pads was carried out by printing lines with a step of 150 μm. With a decrease in the step between the lines, the lines previously deposited by the nanoparticles were destroyed by the flow. The speed of the substrate movement v on the coordinate table relative to the coaxial micronozzle in the process of printing the structures was 10.5 mm/s.

The thickness of the SERS structures formed by gold nanoparticles synthesized in various gaseous media (N_2, Ar + H_2, and He) at various temperatures (24 °C and −183 °C) was measured using an optical 3D profilometer (S neox, Sensofar, Terrassa, Spain).

The Raman spectra of the formed SERS structures were studied using Raman spectroscopy (DXR Raman Microscope, Thermo Fisher, Scientific, Waltham, MA, USA). We chose 1,2-bis(4-pyridyl)ethylene (BPE) as the detectable substance for evaluating the Raman signal amplification by nanoparticles based on publications [39], and after making sure that the BPE spectrum was easily interpreted, the undesirable effect of fluorescence was at an acceptable level, and the destruction of the substance under the action of the laser was quite slow. A 4:1 mixture of 2-butanol and distilled water was used as a solvent for BPE; thus, solutions with concentrations of 10^{-1}, 10^{-2}, 10^{-3}, and 10^{-4} mol/L were

prepared. A solution with a volume of 0.1 µL was applied to the surface with nanoparticles using a pipette dispenser. The sample was then dried for 30 min before the spectrum was measured. At our disposal were radiation sources (lasers) with a wavelength of 532 nm and 780 nm. When choosing a laser and imaging parameters, a series of measurements was carried out, changing the duration of the signal acquisition (exposure, number of frames), the output laser power, the aperture, and the lens so that the signal-to-noise ratio was as high as possible, the signal acquisition time was shorter, and sample degradation was not observed. We chose a laser with a wavelength of 780 nm to compare the efficiency of the surface amplification of the signal on nanostructures obtained under different conditions, since the results of a series of measurements showed that the use of a 780 nm laser makes it possible to reduce the damaging effect on the sample and obtain easily interpretable spectra. The following parameters were set for measurements: laser power of 20 mW, a 10× objective, a circular aperture of 50 µm, a number frames of 5, and a frame exposure of 1 s. When recording the spectra, the result for all images was automatically averaged and processed to reduce the influence of analyte fluorescence on the measurement result.

Thus, in order to measure the thickness of the SERS structures and their further study by Raman spectroscopy, 15 square pads of 3 mm × 3 mm were formed by gold nanoparticles synthesized in various gaseous media (N_2, Ar + H_2 and He) at different temperatures (24 °C and −183 °C) on ceramic substrates made of aluminum oxide for each concentration of the BPE (10^{-2}, 10^{-3}, 10^{-4} mol/L).

3. Results

The morphology and Au nanoparticles size obtained in nitrogen, argon, and helium atmospheres at different synthesis temperatures were studied using a transmission electron microscope (TEM). It was found that the temperature T_{gas} and the synthesis atmosphere have a significant effect both on the size of primary nanoparticles d_p and their agglomerates d_a, and on the solidity of agglomerates φ and the bond strength between primary nanoparticles χ.

Figure 3 shows TEM images of nanoparticles synthesized in a nitrogen atmosphere at temperatures of 24 °C, −111 °C, and −183 °C. It was found that when the synthesis temperature T_{gas} decreases from 24 °C to −183 °C, the average size of primary nanoparticles d_p and agglomerates d_a decreases from 9.4 ± 3.1 nm to 6.6 ± 2.5 nm and from 102 ± 60 nm to 43 ± 26 nm, respectively (Figure 4 and Table 2). This result is due to a decrease in the Brownian motion of nanoparticles with a decrease in the carrier gas temperature T_{gas}. It can be clearly seen from Equations (2) and (3) that with decreasing gas temperature, the coagulation coefficient K decreases, which describes the agglomeration of both primary particles and their agglomerates. Moreover, it has been experimentally and theoretically found that the mass production of nanoparticle synthesis Δm also decreases with decreasing gas temperature T_{gas} (Table 3). This result is explained by the fact that as the gas temperature decreases, a significant fraction of the discharge energy is spent on heating the $c_{ps}(T_m - T_{gas})$ electrodes, while the fraction of energy responsible for the evaporation of the $0.5c_e V^2 - bT_{gas}{}^4 - gk(T_b - T_{gas})$ electrodes decreases (Equation (6)). In turn, a decrease in the mass production m also contributes to a decrease in the agglomeration of nanoparticles, based on Equation (2).

From the analysis of TEM images using Equation (4), it was found that with a decrease in the synthesis temperature, the solidity of nanoparticle agglomerates φ decreases from 92 ± 2% to 76 ± 3%. In other words, the agglomerates become more branched. In this case, the values of the bond strength between the primary nanoparticles synthesized at 24 °C, −111 °C, and −183 °C also decrease χ and amount to 0.5, 0.3, and 0.1, respectively. A clear comparison of the bond strengths between primary nanoparticles is shown in Figure 2. As a result, it can be concluded that the bond strength between primary nanoparticles becomes much weaker with decreasing synthesis temperature.

In this study, a theoretical approach was applied to predict the particle size distribution as a function of the gas temperature T_{gas}. For this purpose, the model of Feng et al. [28]

was used to calculate the sizes of primary nanoparticles and their agglomerates with a lognormal self-conserving size distribution function. Figure 4 shows the experimental and calculated particle size distributions at T_{gas} equal to 24 °C, −111 °C, and −183 °C for primary nanoparticles and their agglomerates. Estimated particle size distributions were constructed using the mathematical expectation (μ) from Equation (2) and the dispersion value (σ) determined by the formula $\sigma = \mu \times GSD$, where GSD is the geometric standard deviation (1.35−1.40).

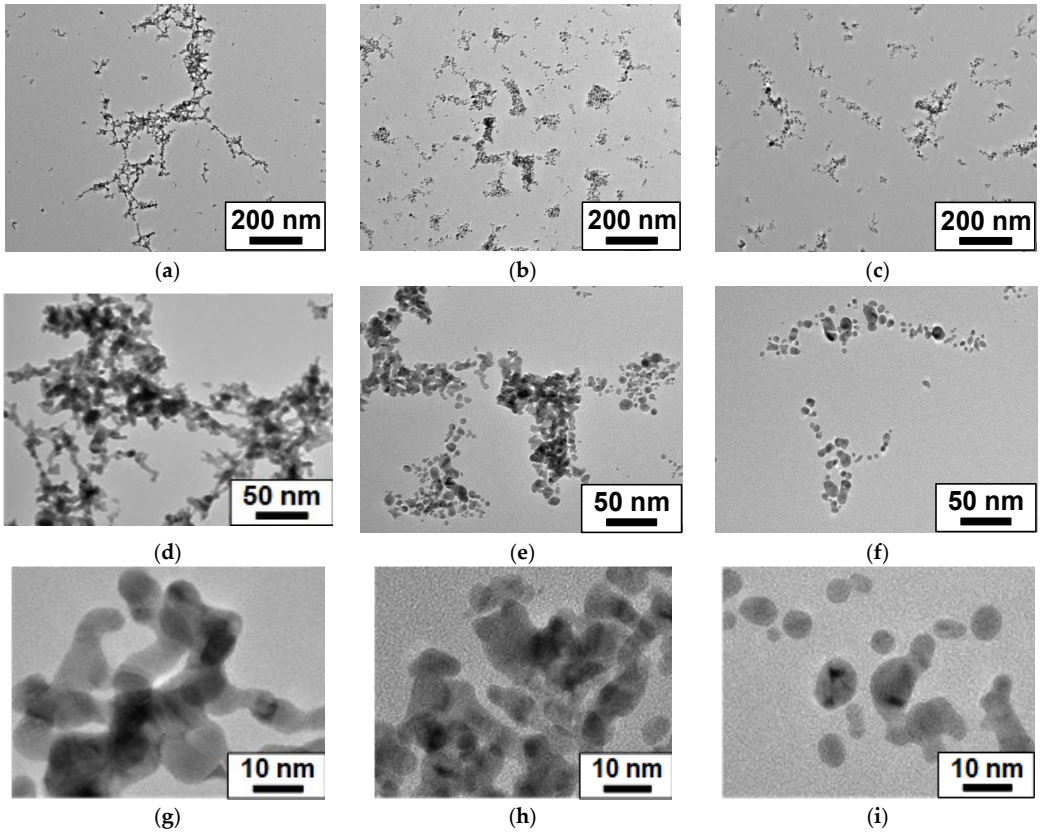

Figure 3. TEM images of Au nanoparticles obtained by spark discharge in chamber with gas temperatures of 24 °C (**a**,**d**,**g**), −111 °C (**b**,**e**,**h**), and −183 °C (**c**,**f**,**i**).

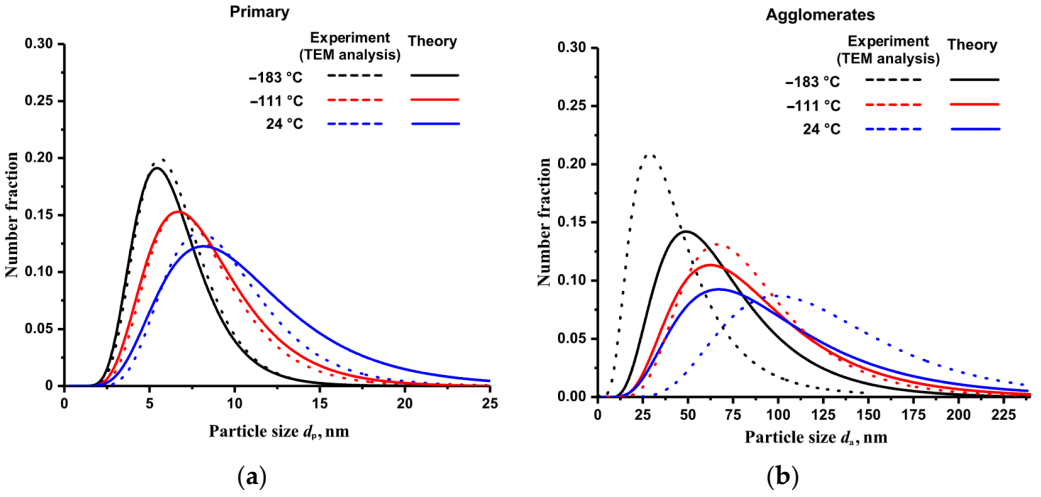

Figure 4. Distribution of primary particles (**a**) and agglomerates (**b**) by size at nitrogen carrier gas temperatures of 24 °C, −111 °C, and −183 °C, plotted from experimental (TEM analysis) and theoretical data.

Table 2. Results of analysis of TEM images of gold nanoparticles obtained in a nitrogen atmosphere at T_{gas} equal to 24 °C, −111 °C, and −183 °C.

Gas temperature T_{gas}, °C	24	−111	−183
Average size of primary nanoparticles d_p, nm	9.4 ± 3.1	7.7 ± 2.6	6.6 ± 2.5
Average size of agglomerates d_a, nm	102 ± 60	76 ± 31	43 ± 26
Solidity φ, %	92 ± 2	86 ± 3	76 ± 3
Relative bond strength χ	0.5	0.3	0.1

Table 3. Mass production of the synthesis of Au nanoparticles depending on the temperature of the carrier gas (nitrogen).

Carrier Gas	Gas Temperature T_{gas}, °C	Mass Production m, mg/h	
		Experimental	Theory
N_2	24	59	53
	−111	52	47
	−183	42	44

Similar to the data presented in Figure 4a, experiments were performed to determine the particle size distribution for nanoparticles obtained in nitrogen, argon, and helium gases (see Figure 5) at room (24 °C) and cryogenic (−183 °C) temperatures, respectively. Figure 5 shows that at these temperatures, the smallest size of primary particles is achieved when using He, and the largest when using N_2. Theoretically, this is explained by an increase in dynamic viscosity during the transition from nitrogen to helium, and hence a decrease in the coagulation coefficient K, see Formula (3).

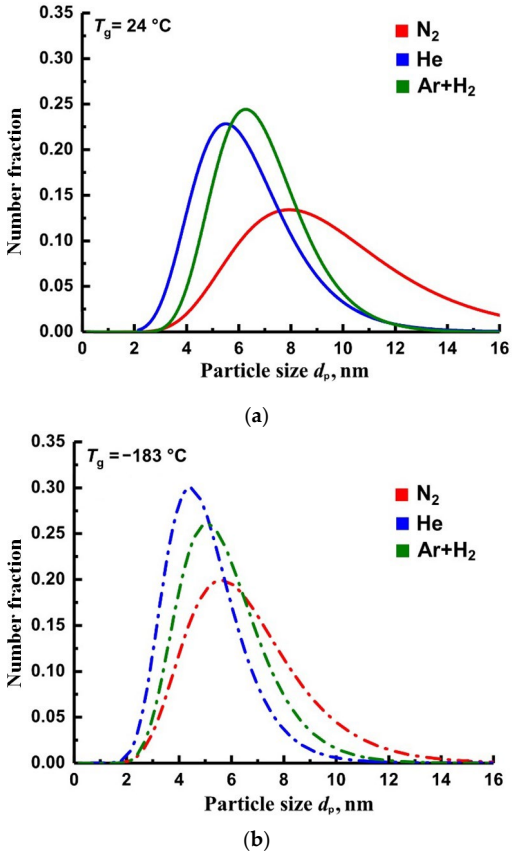

Figure 5. Size distribution of primary Au nanoparticles at temperatures 24 °C (**a**) and –183 °C (**b**) for various type of gases N_2, He, and Ar + H_2.

In order to establish the influence of the type of carrier gas and its temperature T_{gas} on the functional properties of nanoparticles, gold nanostructures were printed from nanoparticles obtained in N_2, He, and Ar + H_2 at temperatures of 24 °C and −183 °C, followed by study on a Raman spectrometer. Figure 6 shows scanning electron microscopy (SEM) images of sections of SERS structures formed from gold nanoparticles [9], which were synthesized in N_2, Ar + H_2, and He atmospheres at temperatures of 24 °C and −183 °C. It should be noted that the structures were formed during the same time interval of about 1 min. The SEM images show that the type of carrier gas significantly affects the density of the formed structures. The densest SERS structures are formed from nanoparticles synthesized in a nitrogen atmosphere, see Figure 5. This result is explained by the fact that agglomerates obtained in nitrogen have large sizes (>100 nm) and, as a result, are deposited much more efficiently through a micronozzle onto a substrate in comparison with small nanoparticles obtained in argon and helium. Moreover, the mass production of nanoparticle synthesis in nitrogen is also higher (42–59 mg/h) than in argon (35–39 mg/h) and helium (18–21 mg/h) (see Table 4). This is also the reason for the formation of denser structures.

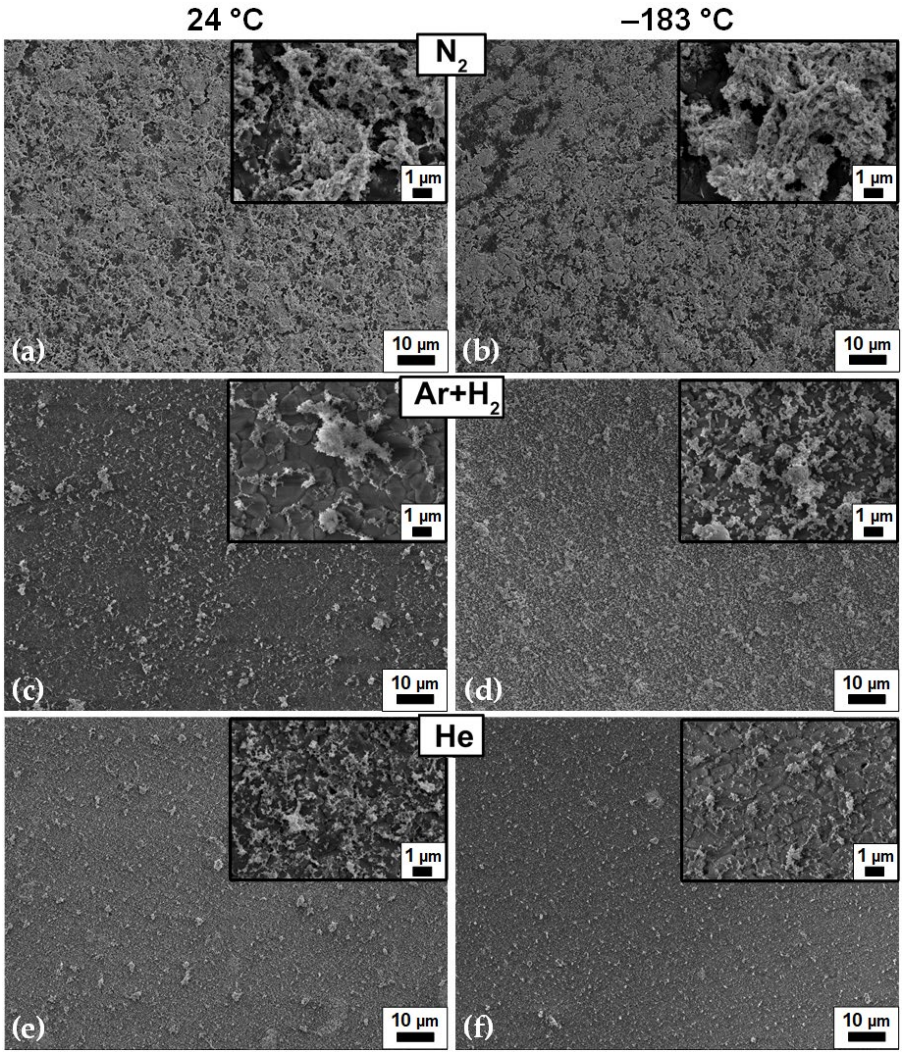

Figure 6. SEM images of SERS structures of Au nanoparticles synthesized in various types of gases (N_2 (**a**,**b**), Ar + H_2 (**c**,**d**), and He (**e**,**f**)) at temperatures of 24 °C and −183 °C and deposited on an aluminum oxide (Al_2O_3) substrate.

Table 4. Mass production of synthesis and thickness of SERS structures obtained by dry aerosol printing. Synthesis of Au nanoparticles was carried out in nitrogen, argon, and helium at 24 °C and −183 °C, respectively.

Atmosphere of Synthesis	Mass Production of Nanoparticle Synthesis, mg/h		Thickness of SERS Structures, µm	
	24 °C	−183 °C	24 °C	−183 °C
N_2	59	42	0.59	0.32
Ar + H_2	39	35	0.28	0.27
He	21	18	0.24	0.19

From the results of measurements of the thicknesses of SERS structures using an optical 3D profilometer, it is also seen that the structures printed with Au nanoparticles synthesized in nitrogen have higher values in comparison with the structures of nanoparticles for argon and helium (Table 4). A similar difference is observed when comparing SERS structures formed from nanoparticles at temperatures of −183 °C and 24 °C. From the analysis of SEM images, it can be seen that at a synthesis temperature of −183 °C, the microstructure of the formed SERS structures is more homogeneous and uniform, while at a synthesis temperature of 24 °C, many individual large particles are deposited on the substrate. Figure 7 shows photographs of SERS structures in the form of 3 mm × 3 mm square pads of gold nanoparticles synthesized in various gases at 24 °C and −183 °C.

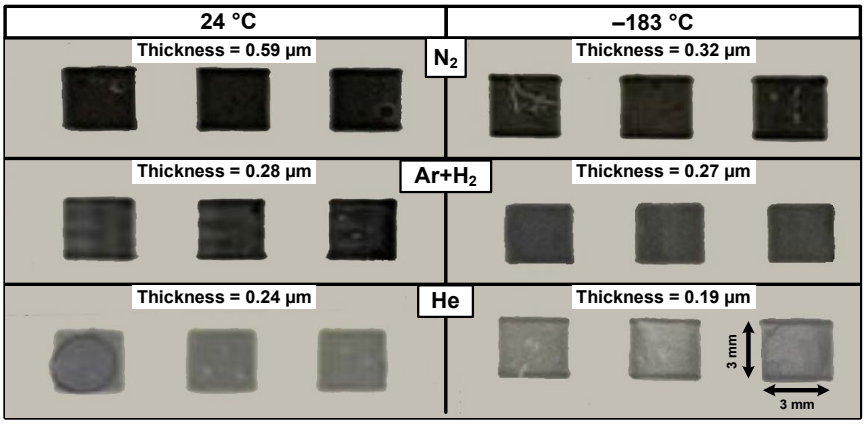

Figure 7. Photographs of SERS structures in the form of square pads 3 mm × 3 mm, formed with different atmospheres and temperatures of nanoparticle synthesis.

Figure 7 shows that thinner and more transparent structures were formed in an argon and helium atmosphere at a low temperature of −183 °C. Figure 8 shows groups of spectra of BPE obtained from gold nanoparticles deposited under different conditions (Figure 8a in a N_2 atmosphere, Figure 8b in a He atmosphere, and Figure 8c in an Ar + H_2 atmosphere). Figure 8d shows the spectra of an alumina substrate (upper), similar to those used for nanoparticle deposition, of a 10^{-1} mol/L BPE solution (middle) supported on alumina, dried after deposition at room temperature under a hood for 30 min, and of a dry BPE powder (bottom spectrum). The characteristic peaks of BPE from a BPE solution dried on alumina substrate with a concentration of 10^{-2} mol/L and less are not distinguishable at the parameters of the spectrum acquisition that we have chosen. The peaks appearing in the spectrum of BPE 10^{-1} in the wavenumber range from 750 cm^{-1} to 850 cm^{-1} are characteristic of the incompletely volatilized butanol, which is part of the BPE solution. For convenience of signal enhancement comparison, the Raman spectra obtained in N_2, He, and Ar + H_2 atmospheres for BPE solutions of the same concentrations (10^{-2}, 10^{-3}, 10^{-4} mol/L) are grouped together. In each group, the scales of the spectra are brought into line.

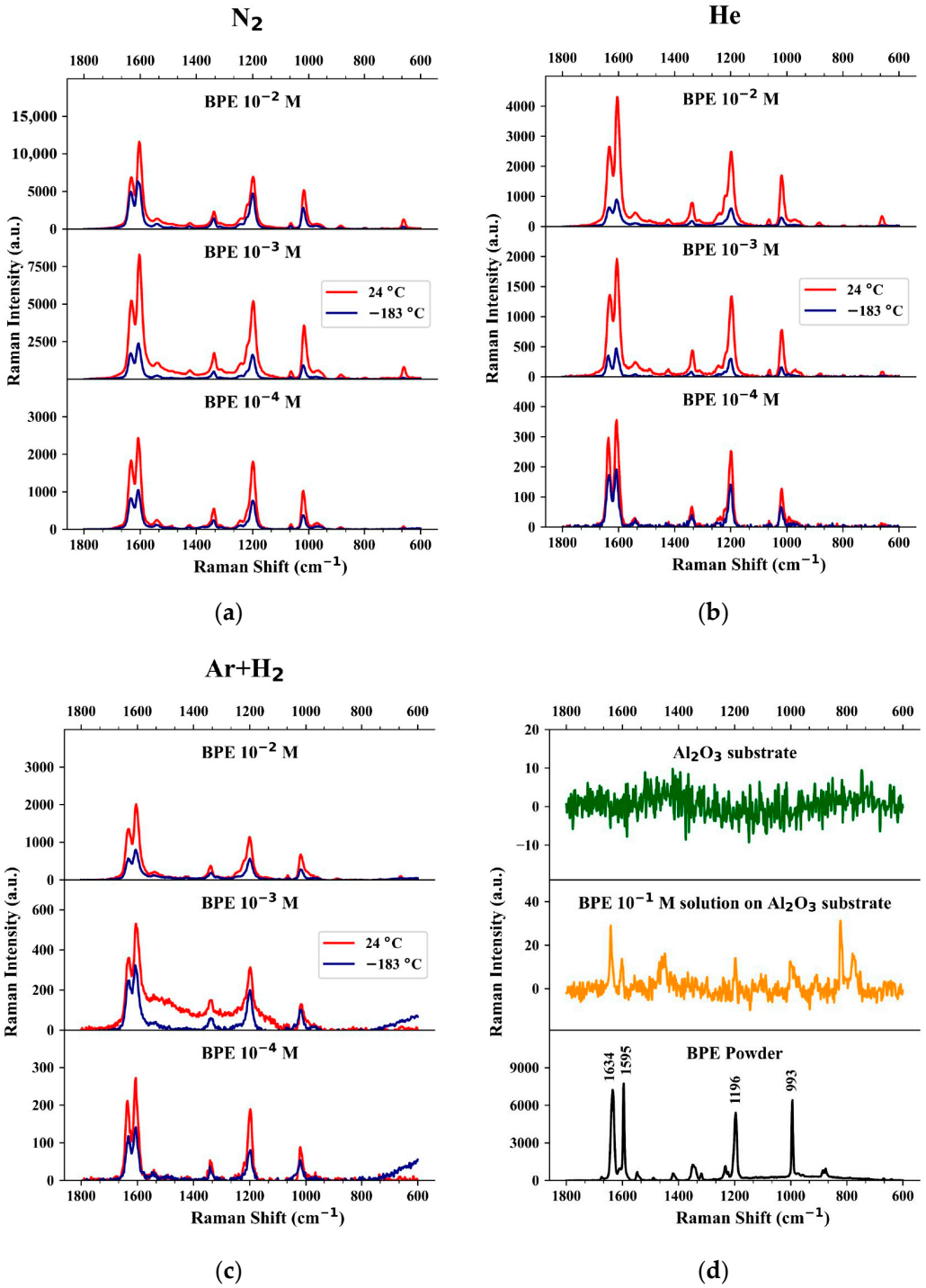

Figure 8. Raman spectra for BPE obtained on SERS structures of Au nanoparticles synthesized in various gaseous media (N_2 (**a**), He (**b**) and Ar + H_2 (**c**)) spectra are scaled in pairs at temperatures of +24 °C (red) and −183 °C (blue), and group of spectra (**d**) of an alumina substrate (green), of a 10^{-1} mol/L BPE solution (orange) supported on alumina, and of a dry BPE powder (black).

The broad peaks appearing in Figure 8c (for nanoparticles synthesized at temperature –183 °C and BPE concentrations of 10^{-3} and 10^{-4} mol/L at wave numbers from 500 cm^{-1} to 700 cm^{-1}) are characteristic for the corresponding gold nanoparticles without applied dye. For each structure and each concentration of BPE, five to seven spectra were obtained, and among them we chose a spectrum with peak heights close to the median. When evaluating the signal amplification, we focused on the characteristic peaks indicated on

the spectrum of dry BPE. The shift of the characteristic peaks of the substance when using different wavelengths of the source (laser) and different amplifying nanostructures for SERS was noted and studied earlier [40–42], and a noticeable shift of the BPE peak in the spectra from nanoparticles relative to dry BPE is presumably due to the peculiarities of the orientation and interaction of BPE molecules with gold nanoparticles. As can be seen from Figure 8, all nanostructures demonstrated the SERS effect, but the amplification intensity for different structures differed significantly. The best result was obtained on gold nanoparticles deposited at T_{gas} = 24 °C in a N_2 atmosphere. The results of Raman spectroscopy show that structures deposited in a N_2 atmosphere enhance the BPE spectrum better than those deposited in a He atmosphere, and particles deposited in an Ar + H_2 atmosphere demonstrate the weakest enhancement. All particles deposited at cryogenic temperature showed a decrease in the intensity of the BPE Raman spectrum in comparison with those deposited at room temperature. This fact is explained by a significant difference in the formed surface density of structures during deposition in different atmospheres and a decrease in the size of agglomerates by more than two times during cryogenic deposition [43–45].

We have estimated the SERS enhancement factor (*EF*) for the BPE molecules adsorbed on gold nanoparticles under study based on the following most widely used definition for the average SERS *EF* [46]:

$$EF = \frac{\left(\frac{I_{SERS}}{N_{surf}}\right)}{\left(\frac{I_{RS}}{N_{vol}}\right)} \quad (7)$$

where I_{SERS} and I_{RS} are the intensities of a particular line of an analyte in the SERS and normal Raman (non-SERS) spectra measured under the same conditions, N_{surf} is the average number of adsorbed molecules in the scattering volume for the SERS experiment, and N_{vol} is the number of molecules in the scattering volume for the non-SERS experiment.

In the calculations, we considered plasmonic nanostructures fabricated by aerosol jet printing with gold nanoparticles synthesized with the use of nitrogen as a carrier gas with no cooling. To estimate the number of analyte molecules probed in the SERS experiment (i.e., N_{surf}), one must know the laser spot size, the average surface density of plasmonic nanoparticles producing the enhancement (i.e., number of particles per unit square of a substrate), the mean size of nanoparticles, and the surface density of analyte molecules adsorbed on nanoparticles.

In the performed experiments, the laser spot size was about 3 μm. Assuming the surface density of primary gold nanoparticles on the substrate to be about 10^{12} cm^{-2} (as estimated from SEM images), their mean size about 9 nm (as estimated from TEM images), surface density of BPE molecules in the monolayer about 3.9 × 10^{14} cm^{-2}, and around 7% surface coverage of the metal [46], approximately 4.8 × 10^6 molecules (N_{surf}) were probed in the SERS experiment. For the non-SERS experiment, the number of molecules (N_{vol}) within the probed volume of a BPE solution (10^{-1} mol/L) dispensed on alumina substrate was estimated at 4.2 × 10^{10}. Substitution of N_{surf}, N_{vol}, and the intensities of a line located at around 1640 cm^{-1} (taken from the typical SERS spectrum acquired on plasmonic nanostructure and the Raman spectrum of BPE solution) into Equation (1) gives an EF equal to about 2 × 10^6.

4. Conclusions

The sealed gas-discharge chamber developed in this work ensured the synthesis of nanoparticles at low temperatures of the carrier gas (Ar + H_2, N_2, and He) down to −183 °C, depending on the level of liquid nitrogen in the chamber. It has been established that as the synthesis temperature decreases from 24 °C to −183 °C, the average size of primary nanoparticles and agglomerates decreases from 9.4 ± 3.1 nm to 6.6 ± 2.5 nm and from 102 ± 60 nm to 43 ± 26 nm, respectively, by reducing the Brownian motion of the nanoparticles. Gold nanoparticles obtained in a spark discharge have been studied to reduce their

agglomeration during synthesis under the influence of carrier gas temperature. Additionally, it was found that with a decrease in the synthesis temperature, the bond strength between primary nanoparticles becomes much weaker and, as a result, the degree of solidity of nanoparticle agglomerates decreases from 92 ± 2% to 76 ± 3%. Aerosol printing of SERS structures from gold nanoparticles was carried out during synthesis in N_2, Ar + H_2, and He atmospheres and at synthesis temperatures of 24 °C and −183 °C for each type of gas. It was found that the enhancement intensity for different types of structures, obtained from the spectra of 1,2-bis(4-pyridyl)ethene from gold nanoparticles, differed significantly. SERS structures formed from nanoparticles at cryogenic temperature demonstrated a decrease in the intensity of the Raman spectrum in comparison with nanoparticles obtained at room temperature. This is due to a decrease in the size of agglomerates and a low surface density of the formed structures during cryogenic deposition. Increasing the surface density by increasing the deposition time of the structures seems to be inappropriate due to the low mass production of spark synthesis in Ar + H_2 and He atmospheres, including when using low temperatures.

Author Contributions: Conceptualization, A.P.; methodology, D.K. and O.V.; investigation, E.K., O.V., M.I., A.M. and D.K.; data curation, A.B., A.M. and I.V.; writing—original draft preparation, A.P.; writing—review and editing, A.E. and P.A.; visualization, A.B.; project administration, A.E., I.V. and V.I. All authors have read and agreed to the published version of the manuscript.

Funding: This research was funded by the Russian Science Foundation grant No. 22-79-10127, https://rscf.ru/project/22-79-10127/ (accessed on 19 January 2023), as part of studying the synthesis of nanoparticles in gas-discharge chambers in liquid nitrogen, and the Ministry of Science and Higher Education of the Russian Federation (state contract No. 075-03-2022-107, project identifier FSMG-2022-0036) as part of scanning and transmission electron microscopy studies. Ivan Volkov and Andrey Musaev acknowledge the Ministry of Science and Higher Education of the Russian Federation (state contract No. 075-03-2022-107, project identifier 0714-2021-0007) for support of surface-enhanced Raman spectroscopy studies.

Data Availability Statement: The data presented in this study are available on request from the corresponding author.

Conflicts of Interest: The authors declare no conflict of interest.

References

1. Feng, J.; Guo, X.; Ramlawi, N.; Pfeiffer, T.V.; Geutjens, R.; Basak, S.; Nirschl, H.; Biskos, G.; Zandbergen, H.W.; Schmidt-Ott, A. Green Manufacturing of Metallic Nanoparticles: A Facile and Universal Approach to Scaling Up. *J. Mater. Chem. A* **2016**, *4*, 11222–11227. [CrossRef]
2. Feng, J.; Chen, D.; Pikhitsa, P.V.; Jung, Y.; Yang, J.; Choi, M. Unconventional Alloys Confined in Nanoparticles: Building Blocks for New Matter. *Matter* **2020**, *3*, 1646–1663. [CrossRef]
3. Snellman, M.; Eom, N.; Ek, M.; Messing, M.E.; Deppert, K. Continuous Gas-Phase Synthesis of Core–Shell Nanoparticles via Surface Segregation. *Nanoscale Adv.* **2021**, *3*, 3041–3052. [CrossRef] [PubMed]
4. El-Aal, M.A.; Seto, T. Spark discharge deposition of au/cu nanoparticles for surface-enhanced Raman scattering. *Surf. Interface Anal.* **2021**, *53*, 824–828. [CrossRef]
5. Palásti, D.J.; Villy, L.P.; Kohut, A.; Ajtai, T.; Geretovszky, Z.; Galbács, G. Laser-Induced Breakdown Spectroscopy Signal Enhancement Effect for Argon Caused by the Presence of Gold Nanoparticles. *Spectrochim. Acta Part B At. Spectrosc.* **2022**, *193*, 106435. [CrossRef]
6. Snellman, M.; Samuelsson, P.; Eriksson, A.; Li, Z.; Deppert, K. On-Line Compositional Measurements of AuAg Aerosol Nanoparticles Generated by Spark Ablation Using Optical Emission Spectroscopy. *J. Aerosol Sci.* **2022**, *165*, 106041. [CrossRef]
7. Jung, W.; Jung, Y.-H.; Pikhitsa, P.V.; Feng, J.; Yang, Y.; Kim, M.; Tsai, H.-Y.; Tanaka, T.; Shin, J.; Kim, K.-Y.; et al. Three-Dimensional Nanoprinting via Charged Aerosol Jets. *Nature* **2021**, *592*, 54–59. [CrossRef]
8. Van Ginkel, H.J.; Vollebregt, S.; Zhang, G.; Schmidt-Ott, A. Mass and density determination of porous nanoparticle films using a quartz crystal microbalance. *Nanotechnology* **2022**, *33*, 485704. [CrossRef]
9. Ramirez Benavides, J.A.; Krasnikov, D.V.; Gubarev, V.V.; Novikov, I.V.; Kondrashov, V.A.; Starkov, A.V.; Krivokorytov, M.S.; Medvedev, V.V.; Gladush, Y.G.; Nasibulin, A. Renewable Single-Walled Carbon Nanotube Membranes for Extreme Ultraviolet Pellicle Applications. *Carbon* **2022**, *198*, 364–370. [CrossRef]
10. Bhowmick, S.; Maisser, A.; Suleimanov, Y.V.; Schmidt-Ott, A.; Biskos, G. Electronic Structure, Stability, and Electrical Mobility of Cationic Silver Oxide Atomic Clusters. *J. Phys. Chem. A* **2022**, *126*, 6376–6386. [CrossRef]

11. Tsantilis, S.; Pratsinis, S.E. Soft- and Hard-Agglomerate Aerosols Made at High Temperatures. *Langmuir* **2004**, *20*, 5933–5939. [CrossRef]
12. Kallay, N.; Žalac, S. Stability of Nanodispersions: A Model for Kinetics of Aggregation of Nanoparticles. *J. Colloid Interface Sci.* **2002**, *253*, 70–76. [CrossRef]
13. Ma, X.; Zare, Y.; Rhee, K.Y. A Two-Step Methodology to Study the Influence of Aggregation/Agglomeration of Nanoparticles on Young's Modulus of Polymer Nanocomposites. *Nanoscale Res. Lett.* **2017**, *12*, 621. [CrossRef]
14. Villy, L.P.; Kohut, A.; Kéri, A.; Bélteki, Á.; Radnóczi, G.; Fogarassy, Z.; Radnóczi, G.Z.; Galbács, G.; Geretovszky, Z. Continuous Spark Plasma Synthesis of Au/Co Binary Nanoparticles with Tunable Properties. *Sci. Rep.* **2022**, *12*, 18560. [CrossRef]
15. Sapountzi, F.M.; Lavorenti, M.; Vrijburg, W.; Dimitriadou, S.; Tyburska-Pueschel, B.; Thüne, P.; Niemantsverdriet, H.; Pfeiffer, T.V.; Tsampas, M.N. Spark Ablation for the Fabrication of PEM Water Electrolysis Catalyst-Coated Membranes. *Catalysts* **2022**, *12*, 1343. [CrossRef]
16. Wojtaszek, K.; Skibińska, K.; Cebula, F.; Tokarski, T.; Escribà-Gelonch, M.; Hessel, V.; Wojnicki, M. Synthesis and Catalytic Studies of Nanoalloy Particles Based on Bismuth, Silver, and Rhenium. *Metals* **2022**, *12*, 1819. [CrossRef]
17. Kohut, A.; Horváth, V.; Pápa, Z.; Vajda, B.; Kopniczky, J.; Galbács, G.; Geretovszky, Z. One-Step Fabrication of Fiber Optic SERS Sensors via Spark Ablation. *Nanotechnology* **2021**, *32*, 395501. [CrossRef]
18. El-Aal, M.A.; Seto, T.; Kumita, M.; Abdelaziz, A.A.; Otani, Y. Synthesis of Silver Nanoparticles Film by Spark Discharge Deposition for Surface-Enhanced Raman Scattering. *Opt. Mater.* **2018**, *83*, 263–271. [CrossRef]
19. Isaac, N.A.; Ngene, P.; Westerwaal, R.J.; Gaury, J.; Dam, B.; Schmidt-Ott, A.; Biskos, G. Optical Hydrogen Sensing with Nanoparticulate Pd–Au Films Produced by Spark Ablation. *Sens. Actuators B Chem.* **2015**, *221*, 290–296. [CrossRef]
20. Isaac, N.A.; Pikaar, I.; Biskos, G. Metal oxide semiconducting nanomaterials for air quality gas sensors: Operating principles, performance, and synthesis techniques. *Microchim. Acta* **2022**, *189*, 196. Available online: https://link.springer.com/article/10.1007/s00604-022-05254-0 (accessed on 19 January 2023). [CrossRef] [PubMed]
21. Zhang, J.; Ahmadi, M.; Fargas, G.; Perinka, N.; Reguera, J.; Lanceros-Méndez, S.; Llanes, L.; Jiménez-Piqué, E. Silver Nanoparticles for Conductive Inks: From Synthesis and Ink Formulation to Their Use in Printing Technologies. *Metals* **2022**, *12*, 234. [CrossRef]
22. Jo, Y.-S.; Lee, H.-J.; Park, H.-M.; Na, T.-W.; Jung, J.-S.; Min, S.-H.; Kim, Y.K.; Yang, S.-M. Chemical Vapor Synthesis of Nonagglomerated Nickel Nanoparticles by In-Flight Coating. *ACS Omega* **2021**, *6*, 27842–27850. [CrossRef] [PubMed]
23. Tabrizi, N.S.; Ullmann, M.; Vons, V.A.; Lafont, U.; Schmidt-Ott, A. Generation of Nanoparticles by Spark Discharge. *J. Nanoparticle Res.* **2009**, *11*, 315–332. [CrossRef]
24. Han, K.; Kim, W.; Yu, J.; Lee, J.; Lee, H.; Woo, C.G.; Choi, M. A Study of Pin-to-Plate Type Spark Discharge Generator for Producing Unagglomerated Nanoaerosols. *J. Aerosol Sci.* **2012**, *52*, 80–88. [CrossRef]
25. Tikhonov, S.S.; Nouraldeen, M.; Khabarov, K.M.; Efimov, A.A.; Ivanov, V.V. Investigation of Laser and Thermal Sintering Processes of Silver Nanoparticles Agglomerates Synthesized by Spark Discharge. *J. Phys. Conf. Ser.* **2021**, *2086*, 012169. [CrossRef]
26. Khabarov, K.; Nouraldeen, M.; Tikhonov, S.; Lizunova, A.; Efimov, A.; Ivanov, V. Modification of Aerosol Gold Nanoparticles by Nanosecond Pulsed-Periodic Laser Radiation. *Nanomaterials* **2021**, *11*, 2701. [CrossRef] [PubMed]
27. Park, K.-T.; Farid, M.M.; Hwang, J. Anti-Agglomeration of Spark Discharge-Generated Aerosols via Unipolar Air Ions. *J. Aerosol Sci.* **2014**, *67*, 144–156. [CrossRef]
28. Feng, J.; Biskos, G.; Schmidt-Ott, A. Toward Industrial Scale Synthesis of Ultrapure Singlet Nanoparticles with Controllable Sizes in a Continuous Gas-Phase Process. *Sci. Rep.* **2015**, *5*, 15788. [CrossRef]
29. Kohut, A. Hydrogen-Assisted Spark Generation of Silver Nanoparticles: The Effect of Hydrogen Content on the Signal Intensity in Surface-Enhanced Raman Spectroscopy. *J. Aerosol Sci.* **2023**, *167*, 106090. [CrossRef]
30. Volkov, I.A.; Simonenko, N.P.; Efimov, A.A.; Simonenko, T.L.; Vlasov, I.S.; Borisov, V.I.; Arsenov, P.V.; Lebedinskii, Y.Y.; Markeev, A.M.; Lizunova, A.A.; et al. Platinum Based Nanoparticles Produced by a Pulsed Spark Discharge as a Promising Material for Gas Sensors. *Appl. Sci.* **2021**, *11*, 526. [CrossRef]
31. Efimov, A.A.; Arsenov, P.V.; Borisov, V.I.; Buchnev, A.I.; Lizunova, A.A.; Kornyushin, D.V.; Tikhonov, S.S.; Musaev, A.G.; Urazov, M.N.; Shcherbakov, M.I.; et al. Synthesis of Nanoparticles by Spark Discharge as a Facile and Versatile Technique of Preparing Highly Conductive Pt Nano-Ink for Printed Electronics. *Nanomaterials* **2021**, *11*, 234. [CrossRef]
32. Jones, F.L. Electrode Erosion by Spark Discharges. *Br. J. Appl. Phys.* **1950**, *1*, 60–65. [CrossRef]
33. Aghajani, S.; Accardo, A.; Tichem, M. Process and Nozzle Design for High-Resolution Dry Aerosol Direct Writing (DADW) of Sub-100 Nm Nanoparticles. *Addit. Manuf.* **2022**, *54*, 102729. [CrossRef]
34. Efimov, A.A.; Potapov, G.N.; Nisan, A.V.; Ivanov, V.V. Controlled Focusing of Silver Nanoparticles Beam to Form the Microstructures on Substrates. *Results Phys.* **2017**, *7*, 440–443. [CrossRef]
35. Efimov, A.A.; Kornyushin, D.V.; Buchnev, A.I.; Kameneva, E.I.; Lizunova, A.A.; Arsenov, P.V.; Varfolomeev, A.E.; Pavzderin, N.B.; Nikonov, A.V.; Ivanov, V.V. Fabrication of Conductive and Gas-Sensing Microstructures Using Focused Deposition of Copper Nanoparticles Synthesized by Spark Discharge. *Appl. Sci.* **2021**, *11*, 5791. [CrossRef]
36. Kornyushin, D.V.; Efimov, A.A.; Buchnev, A.I.; Kameneva, E.I.; Ivanov, V.V. Laser Sintering of Oxidized Copper Nanoparticles Deposited by Dry Aerosol Printing. *J. Phys. Conf. Ser.* **2021**, *2086*, 012019. [CrossRef]
37. Khabarov, K.; Kornyushin, D.; Masnaviev, B.; Tuzhilin, D.; Saprykin, D.; Efimov, A.; Ivanov, V. The Influence of Laser Sintering Modes on the Conductivity and Microstructure of Silver Nanoparticle Arrays Formed by Dry Aerosol Printing. *Appl. Sci.* **2020**, *10*, 246. [CrossRef]

38. Ivanov, V.; Lizunova, A.; Rodionova, O.; Kostrov, A.; Kornyushin, D.; Aybush, A.; Golodyayeva, A.; Efimov, A.; Nadtochenko, V. Aerosol Dry Printing for SERS and Photoluminescence-Active Gold Nanostructures Preparation for Detection of Traces in Dye Mixtures. *Nanomaterials* **2022**, *12*, 448. [CrossRef]
39. Xu, C.H.; Xie, B.; Liu, Y.J.; He, L.B.; Han, M. Optimizing surface-enhanced Raman scattering by template guided assembling of closely spaced silver nanocluster arrays. *Eur. Phys. J. D* **2009**, *52*, 111–114. Available online: https://link.springer.com/article/10.1140/epjd/e2009-00057-1 (accessed on 19 January 2023). [CrossRef]
40. Álvarez-Puebla, R.A. Effects of the Excitation Wavelength on the SERS Spectrum. *J. Phys. Chem. Lett.* **2012**, *3*, 857–866. [CrossRef] [PubMed]
41. Colas, F.J.; Cottat, M.; Gillibert, R.; Guillot, N.; Djaker, N.; Lidgi-Guigui, N.; Toury, T.; Barchiesi, D.; Toma, A.; Di Fabrizio, E.; et al. Red-Shift Effects in Surface Enhanced Raman Spectroscopy: Spectral or Intensity Dependence of the Near-Field? *J. Phys. Chem. C* **2016**, *120*, 13675–13683. [CrossRef]
42. Chong, N.S.; Smith, K.A.; Setti, S.; Ooi, B.G. Application of Gold and Silver Colloidal Nanoparticles for the Surface-Enhanced Raman Spectrometric Analysis of Melamine and 4-Aminobiphenyl. *Int. J. Environ. Technol. Manag.* **2013**, *16*, 3–20. [CrossRef]
43. Wang, R.; He, Z.; Sokolov, A.V.; Kurouski, D. Gap-Mode Tip-Enhanced Raman Scattering on Au Nanoplates of Varied Thickness. *J. Phys. Chem. Lett.* **2020**, *11*, 3815–3820. [CrossRef]
44. Bozhevolnyi, S.I.; Volkov, V.S.; Leosson, K. Localization and Waveguiding of Surface Plasmon Polaritons in Random Nanostructures. *Phys. Rev. Lett.* **2002**, *89*, 186801. [CrossRef] [PubMed]
45. Milekhin, A.G.; Rahaman, M.; Rodyakina, E.E.; Latyshev, A.V.; Dzhagan, V.M.; Zahn, D.R.T. Giant Gap-Plasmon Tip-Enhanced Raman Scattering of MoS2 Monolayers on Au Nanocluster Arrays. *Nanoscale* **2018**, *10*, 2755–2763. [CrossRef] [PubMed]
46. Le Ru, E.C.; Blackie, E.; Meyer, M.; Etchegoin, P.G. Surface Enhanced Raman Scattering Enhancement Factors: A Comprehensive Study. *J. Phys. Chem. C* **2007**, *111*, 13794–13803. [CrossRef]